Enhancement of secondary organic aerosol formation and its oxidation state by SO₂ during photooxidation of 2-methoxyphenol

Changgeng Liu[1,2,a], Tianzeng Chen[1,4,a], Yongchun Liu[3], Jun Liu[1,4], Hong He[1,4,5], Peng Zhang[1,4]

[1]State Key Joint Laboratory of Environment Simulation and Pollution Control, Research Center for Eco-Environmental Sciences, Chinese Academy of Sciences, Beijing 100085, China

[2]School of Biological and Chemical Engineering, Panzhihua University, Panzhihua 617000, China

[3]Beijing Advanced Innovation Center for Soft Matter Science and Engineering, Beijing University of Chemical Technology, Beijing 100029, China

[4]University of Chinese Academy of Sciences, Beijing 100049, China

[5]Center for Excellence in Regional Atmospheric Environment, Institute of Urban Environment, Chinese Academy of Sciences, Xiamen 361021, China

[a]These authors contributed equally to this work and should be considered as co-first authors

Correspondence to: Yongchun Liu (liuyc@buct.edu.cn) and Hong He (honghe@rcees.ac.cn)

Abstract. 2-Methoxyphenol (guaiacol) is derived from the lignin pyrolysis and taken

as a potential tracer for wood smoke emissions. In this work, the effect of SO_2 at

atmospheric levels (0−56 ppbv) on secondary organic aerosol (SOA) formation and its

oxidation state during guaiacol photooxidation was investigated in the presence of

various inorganic seed particles (i.e., NaCl and $(NH_4)_2SO_4$). Without SO_2 and seed

particles, SOA yields ranged from (9.46 ± 1.71) % to (26.37 ± 2.83) % and could be

well expressed by a one-product model. According to the ratio of the average gas-

particle partitioning timescale ($\overline{\tau}_{g-p}$) over the course of experiment to the vapor wall

deposition timescale (τ_{g-w}), the determined SOA yields were underestimated by a factor

of ~2 times. The presence of SO_2 resulted in enhancing SOA yield by 14.04 %−23.65 %.

With $(NH_4)_2SO_4$ and NaCl seed particles, SOA yield was enhanced by 23.07 % and

29.57 %, respectively, which further increased significantly to 29.78 %−53.43 % in the

presence of SO_2, suggesting that SO_2 and seed particles have a synergetic contribution

to SOA formation. The decreasing trend of $\overline{\tau}_{g-p} / \tau_{g-w}$ ratio in the presence of seed

particles and SO_2 suggested that more SOA-forming vapors partitioned into the particle

phase, consequently increasing SOA yields. It should be noted that SO_2 was found to

be in favor of increasing the carbon oxidation state (OS_C) of SOA, indicating that the

functionalization reaction or the partitioning of highly oxidized products into particles

should be more dominant than oligomerization reaction. In addition, the average N/C

ratio of SOA was 0.037, which revealed that NO_x participated in the photooxidation

process, consequently leading to the formation of organic N-containing compounds.

40   The experimental results demonstrate the importance of SO_2 on the formation processes

41   of SOA and organic S-containing compounds, and also are helpful to further understand

42   SOA formation from the atmospheric photooxidation of guaiacol and its subsequent

43   impacts on air quality and climate.

1 Introduction

Biomass burning is considered as one of the major sources of gas and particulate pollutants in the atmosphere (Lauraguais et al., 2014b; Yang et al., 2016). Therefore, it has significant adverse impacts on regional and global air quality (Bari and Kindzierski, 2016; Lelieveld et al., 2001), climate (Chen and Bond, 2010), and human health (Naeher et al., 2007). The chemical species emitted by biomass burning is mainly dependent on fuel source and combustion conditions (O'Neill et al., 2014). Natural wood is composed of cellulose (40−50 wt.%), hemicelluloses (25−35 wt.%), and lignin (18−35 wt.%) (Nolte et al., 2001). During the burning process, lignin pyrolysis could result in the formation of methoxyphenols, mainly including guaiacol (2-methoxyphenol), syringol (2,6-dimethoxyphenol), and their derivatives (Nolte et al., 2001; Schauer et al., 2001). Due to the high emission rate of methoxyphenols (900−4200 mg kg^{-1} wood), methoxyphenols are considered as the potential tracers for wood burning (Hawthorne et al., 1989, 1992; Simoneit et al., 1993).

As a representative type of methoxyphenols, guaiacol mainly exists in the gas phase and is widely found in the atmosphere (Schauer et al., 2001). Its emission factor of wood burning is in the range of 172−279 mg kg^{-1} wood (Schauer et al., 2001). In recent years, the reactivity of gas-phase guaiacol toward OH radicals (Coeur-Tourneur et al., 2010a), NO$_3$ radicals (Lauraguais et al., 2016; Yang et al., 2016), Cl atom (Lauraguais et al., 2014a), and O$_3$ (El Zein et al., 2015) has been investigated, suggesting that its degradation by OH and NO$_3$ radicals might be predominant in the atmosphere.

65   Meanwhile, several studies have reported the significant SOA formation from guaiacol

66   oxidation by OH radicals, produced from the photolysis of the OH precursors (i.e., H_2O_2

67   and CH_3ONO) (Ahmad et al., 2017; Lauraguais et al., 2014b; Yee et al., 2013). However,

68   SOA formation from the photooxidation of guaiacol in the presence of NO_x has not

69   been investigated without adding a direct OH precursor, even though it has been

70   recently reported that the atmospheric level of NO_x could reach up to 200 ppbv in

71   severely polluted atmospheres of China (Li et al., 2017).

72   Although many studies concentrated on the SOA production from the oxidation of

73   volatile organic compounds (VOCs), the reported SOA yields showed high variability

74   for a given precursor (Chu et al., 2016, 2017; Ge et al., 2017a; Lauraguais et al., 2012,

75   2014b; Ng et al., 2007; Sarrafzadeh et al., 2016; Yee et al., 2013). This variability is

76   mainly dependent on the numerous factors, e.g., pre-existing seed particles, SO_2 level,

77   NO_x level, humidity, and temperature. Two of the critical factors are the impacts of pre-

78   existing seed particles and SO_2 level on SOA formation (Chu et al., 2016, 2017; Ge et

79   al., 2017a). In addition, the atmospheric concentration of SO_2 could be up to close 200

80   ppbv in severely polluted atmospheres of China, and SOA from biomass burning and

81   sulfate formation could significantly contribute to severe haze pollution (Li et al., 2017).

82   During the transport process, smoke plumes from biomass burning would be inevitably

83   mixed with suspended particles (e.g., $(NH_4)_2SO_4$ particles), SO_2, and NO_x in the

84   atmosphere. However, the influences of these co-existing pollutants on the

85   transformation of guaiacol and its SOA formation are still unclear. For these reasons,

86   the aim of this work was to investigate the SOA formation from guaiacol

87   photooxidation in the presence of NO_x in a 30 m^3 indoor smog chamber, as well as the

88   effect of SO_2 on SOA fromation with various inorganic seed particles.

89   ## 2   Experimental section

90   ### 2.1   Smog Chamber

91   The photooxidation experiments were performed in a 30 m^3 indoor smog chamber (4

92   m (height) $\times$ 2.5 m (width) $\times$ 3 m (length)), which was built in a temperature-controlled

93   room located at the Research Center for Eco-Environment Sciences, Chinese Academy

94   of Sciences (RCEES-CAS). Its schematic structure is shown in Fig. S1. Briefly, 120

95   UV lamps (365 nm, Philips TL 60/10R) were taken as the light source with a NO_2

96   photolysis rate of 0.55 min^{-1}, which was comparable to the irradiation intensity at noon

97   in Beijing (Chou et al., 2011). A maglev fan installed at the bottom center of the smog

98   chamber was used to mix sufficiently the introduced gas species and seed particles.

99   Temperature (T) and relatively humidity (RH) in the chamber were (302 ±1) K and (39

100   ± 1) %, respectively. Before each experiment, the chamber was flushed by purified dry

101   zero air for ~36 h with a flow rate of 100 L min^{-1} until the particle number concentration

102   in the chamber was lower than 20 cm^{-3}.

103   ### 2.2   Experimental procedures

104   Gas-phase guaiacol was firstly introduced into the chamber by purified dry zero air

105   flowing through the gently heated injector with a known volume of pure liquid guaiacol

106   until guaiacol fully vaporized. Its concentration in the chamber was measured in real-

107   time by a high-resolution proton-transfer reaction time-of-flight mass spectrometer

108   (HR-ToF-PTRMS) (Ionicon Analytik GmbH), and was calibrated by a commercial

109   permeation tube (VICI AG INTERNATIONAL Valco Instruments Co., Inc.). When

110   guaiacol concentration was stable, NO and SO_2 were introduced into the chamber by a

111   mass flow meter using purified dry zero air as the carrier gas. Their concentrations were

112   controlled by the injection time preset through the electromagnetic valve, and were

113   measured by a NO_x analyzer (model 42i-TL, Thermo Fisher Scientific, Inc.) and a SO_2

114   analyzer (model 43i, Thermo Fisher Scientific Inc.), respectively. In this work, the

115   initial ratio (V/V) of guaiacol concentration to NO_x concentration in the chamber was

116   similar in all experiments (~1.2) (Tables 1 and 2). In addition, sodium chloride (NaCl)

117   and ammonium sulfate ($(NH_4)_2SO_4$) were used as the inorganic seeds. The seed aerosols

118   in the chamber were generated by the atomization of a 0.02 M aqueous solution.

119   Through atomization, the size distribution of seed particles peaked at 51−58 nm was

120   achieved, with a number concentration of 10100−11400 cm^{-3} (Table 2). After gas

121   species and seed particles in the chamber were mixed well, the photooxidation

122   experiment was carried out with the fan turned off. In this work, the OH concentrations

123   in the chamber were (1.3−2.2) $\times$ 10^6 molecules cm^{-3}, calculated based on the

124   degradation rate (7.53 $\times 10^{-11}$ cm^3 molecule^{-1} s^{-1}) of guaiacol with OH radicals (Coeur-

125   Tourneur et al., 2010a). The chemicals and gas samples used in this work were

126   described in Supplement.

127   **2.3   Data analysis**

128 The HR-ToF-PTRMS with a time resolution of 1 min was used online to measure the

129 gas phase concentration of guaiacol, and its m/z range was 10−500 in the process of

130 data acquisition. Before data collection, the peaks of the protonated water ($[H_3^{18}O]^+$)

131 and protonated acetone ($[C_3H_7O]^+$) ions at m/z 21.0246 and 59.0491 were used for mass

132 calibration, with the aim to obtain accurate mass determination during experimental

133 process. All data obtained by the HR-ToF-PTRMS were analyzed with the PTR-MS

134 Viewer software (version 3.1.0, IONICON Analytik).

135 An Aerodyne high-resolution time-of-flight aerosol mass spectrometer (HR-ToF-

136 AMS) was applied to online measure the chemical composition of particles and the non-

137 refractory submicron aerosol mass (DeCarlo et al., 2006). For all experiments, the

138 acquisition time of the HR-ToF-AMS was 2 min. The inlet flow rate, ionization

139 efficiency, and particle sizing of the HR-ToF-AMS were calibrated at regular intervals,

140 according to the standard protocols using the size-selected pure ammonium nitrate

141 particles (Drewnick et al., 2005; Jimenez et al., 2003). All date obtained by the HR-

142 ToF-AMS were analyzed by the ToF-AMS analysis toolkit SQUIRREL 1.57I/PIKA

143 1.16I version, in Igor Pro version 6.37. The size distribution and concentration of

144 particles were monitored by a scanning mobility particle sizer (SMPS), which is

145 composed of a differential mobility analyzer (DMA) (model 3082, TSI Inc.) and a

146 condensation particle counter (CPC) (model 3776, TSI Inc.). Assuming that particles

147 are spherical and non-porous, the average particle density could be calculated to be 1.4

148 g cm^{-3} using the equation $\rho=d_{va}/d_m$ (DeCarlo et al., 2004), where d_{va} is the mean vacuum

149 aerodynamic diameter measured by the HR-ToF-AMS and d_m is the mean volume-

150 weighted mobility diameter measured by the SMPS. The mass concentration of

151 particles measured by the HR-ToF-AMS was corrected by the SMPS data in this work

152 using the same method as Gordon et al. (2014). In this work, the wall loss rate (k_{dep}) of

153 $(NH_4)_2SO_4$ particles could be expressed as $k_{dep} = 4.15 \times 10^{-7} \times D_p^{1.89} + 1.39 \times D_p^{-0.88}$

154 (D_p is the particle diameter (nm)), which was measured according to the literature

155 method (Takekawa et al., 2003) and was used to correct the wall loss of SOA. In

156 addition, its wall loss rate was determined at predetermined time intervals, which only

157 had a slight change among different experiments.

158 **2.4 Vapor wall-loss correction**

159 Previous studies have indicated that the losses of SOA-forming vapors to chamber wall

160 can result in the substantial and systematic underestimation of SOA (Zhang et al., 2014,

161 2015). Therefore, SOA yields obtained in this work were also corrected by vapor wall

162 loss. The effect of vapor wall deposition on SOA yields mainly depends on the

163 competition between the uptake of organic vapors by aerosol particles and the chamber

164 wall (Zhang et al., 2015). Thus, the ratio of the average gas-particle partitioning

165 timescale ($\overline{\tau}_{g\text{-}p}$) over the course of experiment to the vapor wall deposition timescale

166 ($\tau_{g\text{-}w}$) could be reasonably used to evaluate the underestimation of SOA yields. The

167 detailed calculation of $\overline{\tau}_{g\text{-}p}$ and $\tau_{g\text{-}w}$ was shown in the Supplement.

168 **3 Results and discussion**

169 **3.1 SOA yields**

170　A series of experiments were conducted at different guaiacol/NO_x concentrations under

171　atmospheric pressure. The experimental conditions and results are shown in Table 1.

172　SOA yield was calculated to be the ratio of SOA mass concentration (M_o, μg m^{-3}) to the

173　consumed guaiacol concentration (Δ[guaiacol], μg m^{-3}) at the end of each experiment

174　(Kang et al., 2007). The results showed that SOA yield was dependent on the initial

175　guaiacol concentration ([Guaiacol]$_0$). Higher precursor concentration would result in

176　higher amount of condensable products, subsequently enhancing SOA formation

177　(Lauraguais et al., 2012). In addition, it should be noted that SOA mass could directly

178　affect the gas/particle partitioning via acting as the adsorption medium of oxidation

179　products, thus higher SOA mass generally leads to higher SOA yield (Lauraguais et al.,

180　2014b).

181　　SOA yield (Y) could be represented by a widely-used semi-empirical model based

182　on the absorptive gas-particle partitioning of semi-volatile products, typically

183　calculated using the following equation (Odum et al., 1996):

184　
$$Y = \sum_i M_o \frac{\alpha_i K_{om,i}}{1 + K_{om,i} M_o} \tag{1}$$

185　where α_i is the mass-based stoichiometric coefficient for the reaction producing the

186　semi-volatile product i, $K_{om,i}$ is the gas-particle partitioning equilibrium constant, and

187　M_o is the total aerosol mass concentration.

188　　The yield curve for guaiacol photooxidation is shown in Fig. 1, obtained by plotting

189　the SOA yield data in Table 1 according to Eq. (1). The yield data were accurately

190　reproduced by a one-product model ($R^2 = 0.97$), while two or more products used in the

191 model did not significantly improve the fitting quality. The obtained values of α_i and

192 $K_{om,i}$ for one-product model were (0.27 $\pm$0.01) and (0.033 $\pm$0.008) $m^3 \mu g^{-1}$, respectively.

193 In previous studies, the one-product model was widely applied to describe SOA yields

194 from the oxidation of aromatic compounds including methoxyphenols (Coeur-Tourneur

195 et al., 2010b; Lauraguais et al., 2012, 2014b). In this work, this simulation suggests that

196 the products in SOA have similar values of α_i and $K_{om,i}$, i.e., the obtained α_i and $K_{om,i}$

197 are the average values. The plot shown in Fig. S2 is the relationship between M_o versus

198 Δ[guaiacol], of which slope (0.28) is slightly higher than α_i value (0.27). This suggests

199 that the formed low-volatile products almost completely partitioned into the particle-

200 phase according to the theoretical partition model (Lauraguais et al., 2012, 2014b).

201 In the previous studies, the significant SOA formation from the OH-initiated

202 reaction of guaiacol has been reported (Lauraguais et al., 2014b; Yee et al., 2013). In

203 this work, SOA yields for guaiacol photooxidation range from (9.46 $\pm$1.71) % to (26.37

204 $\pm$ 2.83) %, shown in Table 1. According to the ratios of $\bar{\tau}_{g\text{-}p} / \tau_{g\text{-}w}$ (0.61−0.93), the

205 determined SOA yields were underestimated by a factor of ~2 times, suggesting that

206 vapor wall loss in the chamber could significantly affect SOA formation. The similar

207 results were reported previously by Zhang et al. (2014), who indicated that SOA yields

208 for toluene photooxidation were substantially underestimated by factors as much as 4

209 times, caused by vapor wall loss. As shown in Fig. 1, the vapor wall-loss corrected SOA

210 yields were in the range of (15.24 $\pm$ 0.85) % to (50.89 $\pm$ 2.87) %, and could also be

211 reproduced by a one-product model (R^2 = 0.96). This range overlaps SOA yields of

212   0.6 %−87 % for guaiacol oxidation under high NO$_x$ condition (~10 ppmv NO), reported

213   by Lauraguais et al. (2014b), using CH$_3$ONO as the OH source. Under low NO$_x$

214   conditions (< 5 ppbv NO), SOA yields for guaiacol oxidation were in the range of

215   44 %−50 %, reported by Yee et al. (2013) using H$_2$O$_2$ as the OH source and (NH$_4$)$_2$SO$_4$

216   as seed particles; they also indicated that high NO$_x$ concentration (> 200 ppbv NO)

217   played an opposite role in SOA formation. Overall, the vapor wall-loss corrected SOA

218   yields in this work are well in agreement with those reported previously (Lauraguais et

219   al., 2014b; Yee et al., 2013), but the determined SOA yields are much lower. Therefore,

220   the effect of vapor wall loss on SOA formation should be seriously taken into account.

221   In addition, the average N/C ratio of SOA for guaiacol photooxidation in the

222   presence of NO$_x$ is 0.037, calculated according to the element analysis by the HR-ToF-

223   AMS. This indicates that NO$_x$ incorporates in guaiacol photooxidation. This

224   phenomenon is well supported by the previous studies, which have reported that the

225   nitro-substituted products are the main products of the OH-initiated reaction of guaiacol

226   in the presence of NO$_x$ (Ahmad et al., 2017; Lauraguais et al., 2014b). The relative low

227   volatility of these products could reasonably contribute to SOA formation (Duporté et

228   al., 2016; Liu et al., 2016a). The average NO^+/NO_2^+ ratio of SOA from guaiacol

229   photooxidation is 4.08, which is higher than that (2.06−2.54) for ammonium nitrate,

230   determined by the HR-ToF-AMS in this work. The possible explanation might be that

231   nitro-organics and organonitrates both exist in SOA (Farmer et al., 2010; Sato et al.,

232   2010). The relative abundance of organic N-containing compounds could be estimated

233　from the average N/C ratio. Assuming that the oxidation products in the SOA retain 7

234　carbon atoms, the yield of organic N-containing compounds is 25.9 %, which is the

235　upper limit due to the possible C－C bond scission during photooxidation process.

236　**3.2　Effect of SO_2 on SOA formation**

237　**3.2.1　SOA yields**

238　In China, atmospheric SO_2 concentration is always in the range of several to dozens of

239　ppbv, while in the severely polluted atmosphere it could be up to close 200 ppbv (Han

240　et al., 2015; Li et al., 2017). In addition, a recent field measurement study has reported

241　that the decrease of biogenic SOA mass concentration in the atmosphere has a positive

242　correlation with SO_2 emission controls (Marais et al., 2017). Therefore, the effect of

243　SO_2 at atmospheric levels on SOA formation from guaiacol photooxidation under

244　atmospheric NO_x conditions was investigated. The experimental conditions and results

245　are shown in Table 2. The formation of SOA, sulfate, and nitrate as a function of SO_2

246　concentration for guaiacol photooxidation is shown in Fig. S3, and the time-series

247　variations in the concentrations of sulfate and nitrate are shown in Fig. S4. The decays

248　of guaiacol, NO_x, and SO_2 are shown in Figs. S5a, S6a, and S7, respectively, which

249　have the similar changing trends for different experiments. As illustrated in Fig. 2, the

250　induction period became shorter with the increase of SO_2 concentration. The similar

251　results caused by SO_2 have also been reported previously (Chu et al., 2016; Liu et al.,

252　2016b). Meanwhile, M_o for the experiment without SO_2 (Exp. 1 in Table 2) increased

253　from (63.62 ± 1.71) to (71.88 ± 1.43) and (78.59 ± 2.06) µg m^{-3}, enhanced by 12.98 %

254   and 23.53 %, respectively, when SO_2 concentration raised from 0 to 33 and 56 ppbv.

255   The corresponding SOA yields were (21.60 ± 1.27) % and (23.42 ± 1.80) %,

256   respectively. The similar results were reported by previous studies (Kleindienst et al.,

257   2006; Lin et al., 2013; Liu et al., 2016b), which observed the significant enhancement

258   of SOA yields for VOCs oxidation and the photochemical aging of gasoline vehicle

259   exhaust in the presence of SO_2.

260   As shown in Fig. 3, $\overline{\tau}_{g\text{-}p} / \tau_{g\text{-}w}$ ratio decreased from 0.82 to 0.71 and 0.61 when

261   SO_2 concentration increased from 0 to 33 and 56 ppbv. It suggests that the formed

262   sulfate via SO_2 oxidation could serve as seed particles (Jaoui et al., 2008) and increase

263   the surface areas of particles (Xu et al., 2016). These roles are favorable to partition

264   more SOA-forming vapors into the particle phase (Zhang et al., 2014), consequently

265   enhancing SOA yields. At the same time, as shown in Fig. S4 and Table 2, the sulfate

266   concentration increased significantly from 7.42 to 17.89 $\mu g \, m^{-3}$ when SO_2 concentration

267   increased from 33 to 56 ppbv. Nevertheless, the particle peak attributed to sulfate

268   formed via SO_2 oxidation was not observed by the SMPS during experimental process

269   due to the quick particle growth in the presence of organic vapors. In this work, it is

270   difficult to completely remove trace of NH_3 from zero air, thus the formed sulfate

271   should be the mixture of H_2SO_4 and $(NH_4)_2SO_4$. The time-series changes in the

272   concentration of ammonium salt at different SO_2 concentrations are shown in Fig. S8.

273   Its concentration increased obviously with increasing SO_2 concentration, suggesting

274   that the more amount of $(NH_4)_2SO_4$ was produced. The similar results have also been

275 reported recently by Chu et al. (2016). In addition, the surface area concentration of

276 aerosol particles at the end time were calculated. As shown in Table 2, the final surface

277 area of aerosol particles formed via guaiacol photooxidation increased from 1.25×10^3

278 to 1.68×10^3 and 2.04×10^3 μm^2 cm^{-3} when SO_2 concentration increased from 0 to 33

279 and 56 ppbv. The increased surface area could be in favor of outcompeting the wall loss

280 for low-volatility vapors produced from guaiacol photooxidation, i.e., more low-

281 volatility vapors would be diverted from wall loss to the particles, consequently

282 increasing SOA yields (Kroll et al., 2007). This is well supported by the decrease of

283 $\overline{\tau}_{g\text{-}p} / \tau_{g\text{-}w}$ ratio with increasing SO_2 concentration, shown in Fig. 3.

284 The time-series changes in the mass concentrations of NO^+ and NO_2^+ are

285 shown in Fig. S9a. The mass concentration of NO^+ increased more quickly than that

286 of NO_2^+, and had a positive correlation with SO_2 concentration. But, compared to the

287 experiment without SO_2, the presence of SO_2 had little impact on NO^+ / NO_2^+ and N/C

288 ratios obtained at the end time, shown in Figs. S9b and S10b, respectively. These ratios

289 indicated that organic N-containing compounds were also produced in this system

290 (Farmer et al., 2010; Sato et al., 2010).

291 **3.2.2 Oxidation state of SOA**

292 The average carbon oxidation state ($OS_C = 2O/C − H/C$) of OA is widely used to

293 represent the oxidation degree of atmospheric OA, because it takes into account the

294 saturation level of carbon atoms in the OA (Kroll et al., 2011). As shown in Table 2,

295 increasing SO_2 concentration (0−56 ppbv, Exps. 1−3) leads to the increase of OS_C

296 (0.11−0.18). The variations in H/C, O/C, and N/C ratios as a function of irradiation time

297 are shown in Fig. S10. In order to further identify the effect of SO_2 on the chemical

298 properties of SOA, positive matrix factorization (PMF) analysis for all AMS data

299 obtained at different SO_2 concentrations over the courses of experiments was carried

300 out. Two factors were obtained from the PMF analysis, and their mass spectra are shown

301 in Fig. 4. The organic mass fraction of m/z 44 (CO_2^+), named f_{44}, was 0.122 for Factor

302 2, which is higher than that (0.094) for Factor 1. Therefore, Factor 2 was tentatively

303 assigned to the more-oxidized SOA, while Factor 1 was the less-oxidized SOA (Ulbrich

304 et al., 2009). During the photooxidation process, these two factors had different

305 variations as a function of irradiation time. As shown in Fig. S11, Factor 1 increased

306 along with the reaction and then decreased, while Factor 2 had an increasing trend.

307 Compared to Exps. 1 and 2 in Table 2, the higher fraction of Factor 2 mass obtained at

308 56 ppbv SO_2 (Exp. 3 in Table 2) suggests that the formed SOA mainly consists of more-

309 oxidized products with relatively low volatility. This is well supported by the time-

310 series variations in the fraction of organic ion groups (CH^+, CHO^+, and CHO_{gt1}^+

311 (containing more than one oxygen atom)) (Fig. S12a), which shows the higher fraction

312 of CHO_{gt1}^+ and lower fraction of CH^+ obtained at higher SO_2 concentration,

313 consequently resulting in higher OS_C of SOA.

314   Previous studies mostly reported that the enhancement of SOA yield in the presence

315 of SO_2 was ascribed to the functionalization and oligomerization reactions (Cao and

316 Jang, 2007; Jaoui et al., 2008 ; Liu et al., 2016b; Xu et al., 2016). If the oligomerization

317 reaction plays a predominant role in the presence of SO_2 which will lead to particle

318 phase H_2SO_4, the carbon number of oligomers will increase but their net O/C or H/C

319 values have little change, consequently resulting in little change in the oxidation state

320 of SOA (Chen et al., 2011). Nevertheless, we observed that SO_2 not only enhanced SOA

321 yields, but also resulted in higher OS_C (Table 2 and Fig. 5). This suggests that the

322 functionalization reaction might be predominant with SO_2, which leads to higher OS_C

323 of products with low molecular weight (MW) (Ye et al., 2018), consequently resulting

324 in an overall increase in OS_C and SOA yields. More recently, Ye et al. (2018) also found

325 the similar results in the ozonolysis of limonene. Fig. S13 shows the differences among

326 the normalized mass spectra of SOA formed at different SO_2 concentrations. As shown

327 in Fig. S13a, the signal fractions from the low-MW species were enhanced significantly

328 in the presence of SO_2, and were much higher than those from the high-MW species

329 ($m/z > 300$). The similar results were also observed in Fig. S13b when increasing SO_2

330 concentration. In other words, SO_2 played a more important role in the formation of

331 organic S-containing compounds and the formation or uptake of low-MW species,

332 compared to the formation of high-MW species (i.e., oligomers) that should be

333 reasonably produced via the acid-catalyzed heterogeneous reactions (Cao and Jang,

334 2007; Jaoui et al., 2008; Liu et al., 2016b; Xu et al., 2016).

335   In this work, assuming that all organic S-containing compounds are organosulfates

336 and have the same response factor and fragmentation as methyl sulfate, the conservative

337 lower-bound concentration of organosulfates was calculated to be in the range of (2.1

338 ± 0.8) to (4.3 ± 1.7) ng m^{-3} using the method described by Huang et al. (2015) shown

339 in the Supplement, and increased with the increase of SO$_2$ concentration. This

340 concentration range is close to those derived from the atmospheric oxidation of

341 polycyclic aromatic hydrocarbons and alkane (Meade et al., 2016; Riva et al., 2015).

342 Fig. S14 is the examples of the ions (i.e., CSO^+, $CH_3SO_2^+$, and $CH_3SO_3^+$) of methyl

343 sulfate obtained at 56 ppbv SO$_2$ (Exp. 3 in Table 2). On the other hand, sulfuric acid

344 formed from SO$_2$ may be favorable for the uptake of water-soluble low-MW species

345 (e.g., small carboxylic acids and aldehydes) and also be helpful to retain them in aerosol

346 phase, which would result in the increase of OS$_C$. This is well supported by the time-

347 series variations in the concentrations of acetic acid at different SO$_2$ concentrations

348 measured by the HR-ToF-PTRMS (Fig. S15a), which shows that acetic acid

349 concentration decreased with the increase of SO$_2$ concentration (0−56 ppbv). These

350 results were in good agreement with those reported by Liggio et al. (2005) and Liu et

351 al. (2010), who observed that the uptake of organic compounds under acidic conditions

352 would be enhanced significantly. Recently, Huang et al. (2016) have also reported that

353 acetic acid is present in SOA formed via α-pinene ozonolysis and its uptake would

354 increase in the presence of seed particles. In addition, Krapf et al. (2016) have indicated

355 that peroxides in SOA are unstable and liable to decompose into volatile compounds,

356 consequently leading to decrease SOA yield and OS$_C$. But, Ye et al. (2018) found that

357 the reactions of SO$_2$ with organic peroxides were the dominant sink of SO$_2$, initiated by

358 the heterogeneous uptake of SO$_2$ under humidity condition. These reactions would

359　result in the formation of organic S-containing compounds, consequently increasing

360　SOA yields and OS_C.

361　**3.3　Effect of inorganic seed particles on SOA formation**

362　Seed particle is one of the critical factors influencing SOA formation (Ge et al., 2017a),

363　thus the effects of inorganic seeds (i.e., NaCl and $(NH_4)_2SO_4$) on SOA formation from

364　guaiacol photooxidation were investigated. As shown in Fig. 6, the presence of

365　inorganic seed particles could accelerate SOA growth rate at the initial stage of

366　photooxidation (i.e., shorten induction period), followed by the decrease of growth rate

367　along with the reaction, because the presence of inorganic seeds could promote the

368　condensation of SOA-forming organic products and consequently increase SOA

369　formation (Yee et al., 2013). The results showed that M_o for the experiment without

370　seed particles (Exp. 1 in Table 2) increased from (63.62 $\pm$ 1.71) to (79.44 $\pm$ 1.86) and

371　(84.91 $\pm$ 2.01) μg m^{-3} (Table 2), enhanced by 24.87 % and 33.46 %, respectively, with

372　$(NH_4)_2SO_4$ and NaCl seed particles. The corresponding SOA yields were (23.31 $\pm$ 1.59) %

373　and (24.54 $\pm$ 1.73) %, respectively. In previous work, the similar results about the

374　enhancements of SOA formation by NaCl and $(NH_4)_2SO_4$ seed particles were reported

375　in the oxidation of VOCs (Ge et al., 2017a, 2017b; Huang et al., 2013, 2017). As shown

376　in Fig. 3, $\overline{\tau}_{g\text{-}p} / \tau_{g\text{-}w}$ ratios with $(NH_4)_2SO_4$ and NaCl seed particles were 0.62 and 0.54,

377　respectively, which suggested that more SOA-forming vapors partitioned into the

378　particle phase in the presence of NaCl seed particles (Zhang et al., 2014), consequently

379　resulting in relatively higher SOA yield.

380   As shown in Table 2 and Fig. 6, the SOA mass concentration in the presence of

381   NaCl seed particles was higher than that in the presence of $(NH_4)_2SO_4$ seed particles.

382   In addition, OS_C of SOA in the presence of NaCl seed particles is 0.29, slightly higher

383   than that (0.20) in the presence of $(NH_4)_2SO_4$ seed particles. Recently, it has been also

384   reported that the presence of $(NH_4)_2SO_4$ and $NaNO_3$ seed particles could enhance

385   significantly the oxidation state of SOA, compared to without seed particles (Huang et

386   al., 2016). In this work, the experimental conditions for seed experiments are almost

387   the same (Table 2), including reactant concentration, temperature, RH, and the number

388   and diameter of seed particles. Therefore, the differences in the yield and oxidation state

389   of SOA were reasonably resulted from the different chemical compositions of SOA in

390   the presence of different inorganic seeds. As shown in Figs. S12b and S12c, compared

391   to $(NH_4)_2SO_4$ seed particles, the higher fraction of CHO_{gt1}^{+} and lower fraction of CH^{+}

392   were obtained with NaCl seed particles, consequently resulting in higher OS_C of SOA.

393   The time-series evolution of O/C, H/C, and N/C ratios is shown in Figs. S16 and S17,

394   which indicate that O/C ratios (0.94−0.99) with NaCl seed particles at the end of

395   experiments are higher than those (0.90−0.93) with $(NH_4)_2SO_4$ seed particles. Fig. 7

396   shows the mass spectra of SOA in the presence of NaCl and $(NH_4)_2SO_4$ seed particles

397   obtained by the HR-ToF-AMS, as well as their difference mass spectrum. As shown in

398   Fig. 7, f_{44} for SOA in the presence of NaCl seed particles was higher than that obtained

399   in the presence of $(NH_4)_2SO_4$ seed particles, while the mass fractions of m/z 15 (CH_3)

400   and 29 (CHO) fragments were both lower. The m/z 44 ion (CO_2^{+}) is mainly contributed

401   from acids or acid-derived species, such as esters (Ng et al., 2011). The higher f_{44} of

402   SOA with NaCl than $(NH_4)_2SO_4$ seed particles suggests that the distribution of highly

403   oxidized small carboxylic acids onto seed particles plays an important role in SOA

404   formation, consequently resulting in higher oxidation state of SOA (Huang et al., 2016;

405   Ng et al., 2011). Compared to $(NH_4)_2SO_4$, the hygroscopicity of NaCl is stronger (Ge

406   et al., 2017a; Gysel et al., 2002). The molar ratio of H_2O to NaCl is about 0.1 at 40 %

407   RH, and water is mainly adsorbed on NaCl particles (Weis and Ewing, 1999). Thus, the

408   greater water content on the particle surface could facilitate the uptake of highly

409   oxidized small carboxylic acids onto NaCl particles, which might explain the higher

410   SOA oxidation state observed in the presence of NaCl seed particles (Huang et al.,

411   2016). As shown in Fig. S15, the concentration of acetic acid in the gas phase with

412   NaCl seed particles was lower than that with $(NH_4)_2SO_4$ seed particles. It suggests that

413   the uptake of acetic acid on NaCl seed particles might be higher than that on $(NH_4)_2SO_4$

414   seed particles under the similar experimental conditions (i.e., NO_x and guaiacol

415   concentrations, temperature, and RH). Moreover, the adsorbed acid products would also

416   generate H^+ ions, which could catalyze heterogeneous reactions to produce more-

417   oxidized products or oligomers with relatively low volatility (Fig. S18), consequently

418   resulting in the enhancement of SOA formation (Huang et al., 2013, 2017; Cao and

419   Jang, 2007; Jaoui et al., 2008; Liu et al., 2016b; Xu et al., 2016).

420   In addition, the possible formation of Cl atoms from the photolysis of nitryl

421   chloride ($ClNO_2 \xrightarrow{hv} Cl + NO_2$, $k_1 = \sim 10^{-4}$ s^{-1}) (Mielke et al., 2011) and the reaction

422 of OH radical with Cl^- ($Cl^- + OH \rightarrow Cl + OH^-$, $k_2 = \sim 10^9$ M^{-1} s^{-1}) (Fang et al., 2014)

423 would also initiate a series of reactions to oxidize SOA composition, which might be

424 another reason for higher OS_C observed with NaCl seed particles. According to the rate

425 constant (10^9 M^{-1} s^{-1}) (Fang et al., 2014), the uptake coefficient (3.4×10^{-3}) of OH

426 radicals on NaCl particles (Park et al., 2008), and the concentrations of OH radicals and

427 Cl^-, the concentration of Cl atoms produced from the reaction of OH radical with Cl^-

428 was estimated to be less than 38 molecules cm^{-3}, which was much higher than that from

429 the photolysis of $ClNO_2$ due to the slow photolysis rate constant of $\sim 10^{-4}$ s^{-1} (Mielke

430 et al., 2011). Compared to OH concentration in the chamber, the oxidation of SOA

431 composition by Cl atoms should be insignificant.

432 **3.4 Synergetic effect of SO_2 and inorganic seed particles on SOA formation**

433 According to the former results obtained in this work, it is clearly known that SO_2 and

434 inorganic seed particles both have a positive role in enhancing SOA formation.

435 Therefore, their possible synergetic effects on SOA formation were investigated.

436 Considering the experiments performed under the comparable conditions (Table 2), the

437 results should be reasonably reliable. The decays of guaiacol, NO_x, and SO_2 are shown

438 in Figs. S5, S6, and S7, respectively, which have the similar changing trends for

439 different experiments. Fig. S19 shows the time-series evolution in the sulfate

440 concentration in the presence of different SO_2 concentrations and seed particles, which

441 indicates that sulfate concentration is dependent on SO_2 concentration. As shown in Fig.

442 8, the addition of SO_2 into the chamber in the presence of inorganic seed particles

443   significantly promoted SOA formation from guaiacol photooxidation, but had an

444   ignorable impact on the induction period. When SO_2 concentration raised from 0 to 30

445   and 54 ppbv in the presence of NaCl seed particles, M_o increased from (84.91 $\pm$ 2.01)

446   to (90.89 $\pm$ 2.28) and (98.86 $\pm$ 2.11) $\mu g\ m^{-3}$, enhanced by 7.04 % and 16.43 %,

447   respectively, and the corresponding SOA yields were (26.78 $\pm$ 1.97) % and (29.06 $\pm$

448   1.82) %. For $(NH_4)_2SO_4$ seed particles, M_o increased from (79.44 $\pm$ 1.86) to (84.35 $\pm$

449   2.09) for 33 ppbv SO_2 and (89.92 $\pm$ 2.31) $\mu g\ m^{-3}$ for 54 ppbv SO_2, enhanced by 6.18 %

450   and 13.19 %, respectively, and the corresponding SOA yields were (24.58 $\pm$ 1.78) %

451   and (26.37 $\pm$ 1.98) %. As shown in Fig. 3, $\overline{\tau}_{g\text{-}p} / \tau_{g\text{-}w}$ ratio had a decreasing trend when

452   increasing SO_2 concentration in the presence of seed particles, suggesting that the

453   underestimation of SOA yields caused by vapor wall loss was weakened significantly

454   because of the additional sulfate formed from SO_2 oxidation. Thus, inorganic seed

455   particles and SO_2 have a synergestic effect on SOA formation.

456   As shown in Table 2 and Fig. 5, it should be noted that OS_C of SOA increased in

457   the presence of SO_2, which was well supported by the time-series variations in H/C,

458   O/C, and N/C ratios at different SO_2 concentrations with NaCl and $(NH_4)_2SO_4$ as seed

459   particles, shown in Figs. S16 and S17. In addition, as shown in Figs. S12b and S12c,

460   the higher fraction of CHO_{gt1}^{+} and lower fraction of CH^{+} were obtained at higher SO_2

461   concentration, consequently resulting in higher OS_C of SOA. Fig. S20 shows the mass

462   spectra of SOA with NaCl and $(NH_4)_2SO_4$ as seed particles at different SO_2

463   concentrations obtained by the HR-ToF-AMS. As illustrated in Fig. S20, SO_2 addition

464   was in favor of increasing the value of f_{44}, suggesting that more products with higher

465   OS_C are produced by the functionalization reaction (Ye et al., 2018). Meanwhile, Table

466   2 shows that the final surface area of aerosol particles increased in the presence of SO_2,

467   which played a positive role in diverting more low-volatility vapors from wall loss to

468   the particles, consequently enhancing SOA yields (Kroll et al., 2007). In addition, the

469   presence of inorganic seeds could promote the condensation of SOA-forming organic

470   products and the heterogeneous uptake of SO_2 (Yee et al., 2013), providing favorable

471   conditions for the following reactions. Meanwhile, the higher hygroscopicity of NaCl

472   than $(NH_4)_2SO_4$ might be helpful to dissolve more acid substances on NaCl particle

473   surface (e.g., H_2SO_4 and organic acid), especially in the presence of SO_2. This

474   hypothesis could be supported by the variations in acetic acid concentration in the

475   presence of different seed particles and SO_2 concentrations (Fig. S15), which shows

476   that acetic acid concentration decreased with the increase of SO_2 concentration (0−54

477   ppbv). The dissolved acid compounds might be helpful to catalyze heterogeneous

478   reactions (Cao and Jang, 2007; Huang et al., 2013, 2017; Jaoui et al., 2008; Liu et al.,

479   2016b; Xu et al., 2016). Figs. S21 and S22 show the differences among the normalized

480   mass spectra of SOA formed at different SO_2 concentrations with various seed particles.

481   The results indicated that the signal fractions from the low-MW species increased

482   significantly in the presence of SO_2, and were much higher than those from the high-

483   MW species ($m/z > 300$). Compared to Exps. 2 and 3 in Table 2 with no seed particles,

484   the conservative lower-bound concentrations of organosulfates formed with seed

485   particles were similar and in the range of (2.2 ±0.7) to (4.6 ±1.8) ng m^{-3}, which might

486   be caused by the similar SO_2 concentrations applied for experiments. With NaCl and

487     $(NH_4)_2SO_4$ as seed particles, SOA yields and OS_C both increased with the increase of

488   SO_2, suggesting that the functionalization reaction should be more dominant than

489   oligomerization reaction during photooxidation process.

4   Conclusions and atmospheric implications

491   In this work, SOA formation from guaiacol photooxidation in the presence of NO_x was

492   investigated in a 30 m^3 smog chamber. SOA yields for guaiacol photooxidation were in

493   the range of (9.46 ±1.71) % to (26.37 ±2.83) %, and could be expressed well by a one-

494   product model. These yields were underestimated by a factor of ~2 times according to

495     $\overline{\tau}_{g\text{-}p} / \tau_{g\text{-}w}$ ratios. The presence of SO_2 could increase SOA yield and OS_C, indicating

496   that the functionalization reaction should be more dominant than oligomerization

497   reaction. Meanwhile, the similar effect of SO_2 was also observed with NaCl and

498     $(NH_4)_2SO_4$ seed particles. But, SOA yield and OS_C in the presence of NaCl seed

499   particles were both slightly higher than those in the presence of $(NH_4)_2SO_4$ seed

500   particles. In addition, the results indicated the synergetic contribution of SO_2 and

501   inorganic seed particles to SOA formation. The decreasing trend of $\overline{\tau}_{g\text{-}p} / \tau_{g\text{-}w}$ ratio in

502   the presence of seed particles and SO_2 suggested that more SOA-forming vapors

503   partitioned into the particle phase, consequently increasing SOA yields. The average

504   N/C ratio (0.037) of SOA suggested that NO_x participated in the process of guaiacol

505   photooxidation, resulting in the formation of organic N-containing compounds.

506   The significant SOA formation from guaiacol photooxidation at the atmospheric

507   levels of SO_2 and NO_x in this work suggests that more attention is necessary on the

508   SOA formation from biomass burning and its subsequent effects on haze evolution,

509   especially in China with nationwide biomass burning, because recent studies have

510   indicated that SOA formed from biomass burning plays an important role in haze

511   pollution in China (Ding et al., 2017; Li et al., 2017). In addition, the results imply that

512   the oxidation of SO_2 and VOCs are tightly coupled, and SO_2 has a direct impact on the

513   physics and chemistry of SOA formation. Although guaiacol concentrations in the

514   chamber study are higher than those in the ambient atmosphere, the results obtained in

515   this work could provide new information for SOA formation from the photooxidation

516   of methoxyphenols, and might be useful for SOA modeling, especially for air quality

517   simulation modeling of the specific regions experiencing serious pollution caused by

518   fine particulate matter. In addition, the results would help to further understand the

519   photochemical aging process of smoke plumes from biomass burning in the atmosphere.

520   **Data availability**

521   The experimental data are available upon request to the corresponding authors.

522   **Author contributions**

523   CL, TC, YL, and HH designed the research and wrote the paper. CL, TC, and JL

524   performed the experiments. CL, TC, YL, JL, HH, and PZ carried out the data analysis.

525   All authors contributed to the final paper.

Competing interests

The authors declare that they have no conflict of interest.

Acknowledgements

References

Ahmad, W., Coeur, C., Tomas, A., Fagniez, T., Brubach, J.-B., and Cuisset, A.: Infrared spectroscopy of secondary organic aerosol precursors and investigation of the hygroscopicity of SOA formed from the OH reaction with guaiacol and syringol, Appl. Opt., 56, E116-E122, https://doi.org/10.1364/ao.56.00e116, 2017.

Bari, M. A., and Kindzierski, W. B.: Fine particulate matter (PM2.5) in Edmonton, Canada: Source apportionment and potential risk for human health, Environ. Pollut., 218, 219-229, https://doi.org/10.1016/j.envpol.2016.06.014, 2016.

Cao, G., and Jang, M.: Effects of particle acidity and UV light on secondary organic aerosol formation from oxidation of aromatics in the absence of NO_x, Atmos. Environ., 41, 7603-7613, https://doi.org/10.1016/j.atmosenv.2007.05.034, 2007.

Chen, Q., Liu, Y., Donahue, N. M., Shilling, J. E., and Martin S. T.: Particle-phase chemistry of secondary organic material: Modeled compared to measured O:C and H:C elemental ratios provide constraints, Environ. Sci. Technol., 45, 4763-4770, https://doi.org/10.1021/es104398s, 2011.

553 Chen, Y., and Bond, T. C.: Light absorption by organic carbon from wood combustion,
554   Atmos. Chem. Phys., 10, 1773-1787, https://doi.org/10.5194/acp-10-1773-2010,
555   2010.

556 Chou, C. C. K., Tsai, C. Y., Chang, C. C., Lin, P. H., Liu, S. C., and Zhu, T.:
557   Photochemical production of ozone in Beijing during the 2008 Olympic Games,
558   Atmos. Chem. Phys., 11, 9825-9837, https://doi.org/10.5194/acp-11-9825-2011,
559   2011.

560 Chu, B., Zhang, X., Liu, Y., He, H., Sun, Y., Jiang, J., Li, J., and Hao, J.: Synergetic
561   formation of secondary inorganic and organic aerosol: Effect of SO_2 and NH_3 on
562   particle formation and growth, Atmos. Chem. Phys., 16, 14219-14230,
563   https://doi.org/10.5194/acp-16-14219-2016, 2016.

564 Chu, B., Liggio, J., Liu, Y., He, H., Takekawa, H., Li, S.-M., and Hao, J.: Influence of
565   metal-mediated aerosol-phase oxidation on secondary organic aerosol formation
566   from the ozonolysis and OH-oxidation of α-pinene, Sci. Rep., 7, 40311,
567   https://doi.org/10.1038/srep40311, 2017.

568 Coeur-Tourneur, C., Cassez, A., and Wenger, J. C.: Rate coefficients for the gas-phase
569   reaction of hydroxyl radicals with 2-methoxyphenol (guaiacol) and related
570   compounds, J. Phys. Chem. A, 114, 11645-11650,
571   https://doi.org/10.1021/jp1071023, 2010a.

572 Coeur-Tourneur, C., Foulon, V., and Lareal, M.: Determination of aerosol yields from
573   3-methylcatechol and 4-methylcatechol ozonolysis in a simulation chamber,
574   Atmos. Environ., 44, 852-857, https://doi.org/10.1016/j.atmosenv.2009.11.027,
575   2010b.

576 DeCarlo, P. F., Slowik, J. G., Worsnop, D. R., Davidovits, P., and Jimenez, J. L.: Particle
577   morphology and density characterization by combined mobility and aerodynamic
578   diameter measurements. Part 1: Theory, Aerosol Sci. Technol., 38, 1185-1205,
579   https://doi.org/10.1080/027868290903907, 2004.

580 DeCarlo, P. F., Kimmel, J. R., Trimborn, A., Northway, M. J., Jayne, J. T., Aiken, A. C.,
581   Gonin, M., Fuhrer, K., Horvath, T., Docherty, K. S., Worsnop, D. R., and Jimenez,
582   J. L.: Field-deployable, high-resolution, time-of-flight aerosol mass spectrometer,
583   Anal. Chem., 78, 8281-8289, https://doi.org/10.1021/ac061249n, 2006.

584 Ding, X., Zhang, Y.-Q., He, Q.-F., Yu, Q.-Q., Wang, J.-Q., Shen, R.-Q., Song, W., Wang,
585   Y.-S., and Wang, X.-M.: Significant increase of aromatics-derived secondary
586   organic aerosol during fall to winter in China, Environ. Sci. Technol., 51, 7432-
587   7441, https://doi.org/10.1021/acs.est.6b06408, 2017.

588 Drewnick, F., Hings, S. S., DeCarlo, P., Jayne, J. T., Gonin, M., Fuhrer, K., Weimer, S.,
589   Jimenez, J. L., Demerjian, K. L., Borrmann, S., and Worsnop, D. R.: A new time-
590   of-flight aerosol mass spectrometer (TOF-AMS)-instrument description and first
591   field deployment, Aerosol Sci. Technol., 39, 637-658,
592   https://doi.org/10.1080/02786820500182040, 2005.

593 Duporté, G., Parshintsev, J., Barreira, L. M. F., Hartonen, K., Kulmala, M., and
594   Riekkola, M.-L.: Nitrogen-containing low volatile compounds from

595   pinonaldehyde-dimethylamine reaction in the atmosphere: A laboratory and field
596   study, Environ. Sci. Technol., 50, 4693-4700,
597   https://doi.org/10.1021/acs.est.6b00270, 2016.

598   El Zein, A., Coeur, C., Obeid, E., Lauraguais, A., and Fagniez, T.: Reaction kinetics of
599   catechol (1,2-benzenediol) and guaiacol (2-methoxyphenol) with ozone, J. Phys.
600   Chem. A, 119, 6759-6765, https://doi.org/10.1021/acs.jpca.5b00174, 2015.

601   Fang, J., Fu, Y., and Shang, C.: The roles of reactive species in micropollutant
602   degradation in the UV/free chlorine system, Environ. Sci. Technol., 48, 1859-1868,
603   https://doi.org/10.1021/es4036094, 2014.

604   Farmer, D. K., Matsunaga, A., Docherty, K. S., Surratt, J. D., Seinfeld, J. H., Ziemann,
605   P. J., and Jimenez, J. L.: Response of an aerosol mass spectrometer to
606   organonitrates and organosulfates and implications for atmospheric chemistry,
607   Proc. Natl. Acad. Sci. U. S. A., 107, 6670-6675,
608   https://doi.org/10.1073/pnas.0912340107, 2010.

609   Ge, S., Xu, Y., and Jia, L.: Effects of inorganic seeds on secondary organic aerosol
610   formation from photochemical oxidation of acetone in a chamber, Atmos. Environ.,
611   170, 205-215, https://doi.org/10.1016/j.atmosenv.2017.09.036, 2017a.

612   Ge, S., Xu, Y., and Jia, L.: Secondary organic aerosol formation from propylene
613   irradiations in a chamber study, Atmos. Environ., 157, 146-155,
614   https://doi.org/10.1016/j.atmosenv.2017.03.019, 2017b.

615   Gordon, T. D., Presto, A. A., Nguyen, N. T., Robertson, W. H., Na, K., Sahay, K. N.,
616   Zhang, M., Maddox, C., Rieger, P., Chattopadhyay, S., Maldonado, H., Maricq, M.
617   M., and Robinson, A. L.: Secondary organic aerosol production from diesel
618   vehicle exhaust: impact of aftertreatment, fuel chemistry and driving cycle, Atmos.
619   Chem. Phys., 14, 4643-4659, https://doi.org/10.5194/acp-14-4643-2014, 2014.

620   Gysel, M., Weingartner, E., and Baltensperger, U.: Hygroscopicity of aerosol particles
621   at low temperatures. 2. Theoretical and experimental hygroscopic properties of
622   laboratory generated aerosols, Environ. Sci. Technol., 36, 63-68,
623   https://doi.org/10.1021/es010055g, 2002.

624   Han, T., Liu, X., Zhang, Y., Qu, Y., Zeng, L., Hu, M., and Zhu, T.: Role of secondary
625   aerosols in haze formation in summer in the Megacity Beijing, J. Environ. Sci., 31,
626   51-60, https://doi.org/10.1016/j.jes.2014.08.026, 2015.

627   Hawthorne, S. B., Krieger, M. S., Miller, D. J., and Mathiason, M. B.: Collection and
628   quantitation of methoxylated phenol tracers for atmospheric pollution from
629   residential wood stoves, Environ. Sci. Technol., 23, 470-475,
630   https://doi.org/10.1021/es00181a013, 1989.

631   Hawthorne, S. B., Miller, D. J., Langenfeld, J. J., and Krieger, M. S.: PM10 high-
632   volume collection and quantitation of semivolatile and nonvolatile phenols,
633   methoxylated phenols, alkanes, and polycyclic aromatic hydrocarbons from winter
634   urban air and their relationship to wood smoke emissions, Environ. Sci. Technol.,
635   26, 2251-2262, https://doi.org/10.1021/es00035a026, 1992.

636   Huang, D. D., Li, Y. J., Lee, B. P., and Chan, C. K.: Analysis of organic sulfur

compounds in atmospheric aerosols at the HKUST supersite in Hong Kong using HR-ToF-AMS, Environ. Sci. Technol., 49, 3672-3679, https://doi.org/10.1021/es5056269, 2015.

Huang, D. D., Zhang, X., Dalleska, N. F., Lignell, H., Coggon, M. M., Chan, C.-M., Flagan, R. C., Seinfeld, J. H., and Chan, C. K.: A note on the effects of inorganic seed aerosol on the oxidation state of secondary organic aerosol-alpha-Pinene ozonolysis, J. Geophys. Res.-Atmos., 121, 12476-12483, https://doi.org/10.1002/2016jd025999, 2016.

Huang, M., Hao, L., Gu, X., Hu, C., Zhao, W., Wang, Z., Fang, L., and Zhang, W.: Effects of inorganic seed aerosols on the growth and chemical composition of secondary organic aerosol formed from OH-initiated oxidation of toluene, J. Atmos. Chem., 70, 151-164, https://doi.org/10.1007/s10874-013-9262-9, 2013.

Huang, M., Hao, L., Cai, S., Gu, X., Zhang, W., Hu, C., Wang, Z., Fang, L., and Zhang, W.: Effects of inorganic seed aerosols on the particulate products of aged 1,3,5-trimethylbenzene secondary organic aerosol, Atmos. Environ., 152, 490-502, https://doi.org/10.1016/j.atmosenv.2017.01.010, 2017.

Jaoui, M., Edney, E. O., Kleindienst, T. E., Lewandowski, M., Offenberg, J. H., Surratt, J. D., and Seinfeld, J. H.: Formation of secondary organic aerosol from irradiated α-pinene/toluene/NO$_x$ mixtures and the effect of isoprene and sulfur dioxide, J. Geophys. Res.-Atmos., 113, D09303, https://doi.org/10.1029/2007jd009426, 2008.

Jimenez, J. L., Jayne, J. T., Shi, Q., Kolb, C. E., Worsnop, D. R., Yourshaw, I., Seinfeld, J. H., Flagan, R. C., Zhang, X., Smith, K. A., Morris, J. W., and Davidovits, P.: Ambient aerosol sampling using the Aerodyne Aerosol Mass Spectrometer, J. Geophys. Res.-Atmos., 108, 8425, https://doi.org/10.1029/2001JD001213, 2003.

Kang, E., Root, M. J., Toohey, D. W., and Brune, W. H.: Introducing the concept of Potential Aerosol Mass (PAM), Atmos. Chem. Phys., 7, 5727-5744, https://doi.org/10.5194/acp-7-5727-2007, 2007.

Kleindienst, T. E., Edney, E. O., Lewandowski, M., Offenberg, J. H., and Jaoui, M.: Secondary organic carbon and aerosol yields from the irradiations of isoprene and α-pinene in the presence of NO$_x$ and SO$_2$, Environ. Sci. Technol., 40, 3807-3812, https://doi.org/10.1021/es052446r, 2006.

Krapf, M., El Haddad, I., Bruns, E. A., Molteni, U., Daellenbach, K. R., Prevot, A. S. H., Baltensperger, U., and Dommen, J.: Labile peroxides in secondary organic aerosol, Chem, 1, 603-616, https://doi.org/10.1016/j.chempr.2016.09.007, 2016.

Kroll, J. H., Chan, A. W. H., Ng, N. L., Flagan, R. C., andSeinfeld, J. H.: Reactions of semivolatile organics and their effects on secondary organic aerosol formation, Environ. Sci. Technol., 41, 3545-3550, https://doi.org/10.1021/es062059x, 2007.

Kroll, J. H., Donahue, N. M., Jimenez, J. L., Kessler, S. H., Canagaratna, M. R., Wilson, K. R., Altieri, K. E., Mazzoleni, L. R., Wozniak, A. S., Bluhm, H., Mysak, E. R., Smith, J. D., Kolb, C. E., and Worsnop, D. R.: Carbon oxidation state as a metric for describing the chemistry of atmospheric organic aerosol, Nature Chem., 3, 133-139, https://doi.org/10.1038/nchem.948, 2011.

Lauraguais, A., Coeur-Tourneur, C., Cassez, A., and Seydi, A.: Rate constant and secondary organic aerosol yields for the gas-phase reaction of hydroxyl radicals with syringol (2,6-dimethoxyphenol), Atmos. Environ., 55, 43-48, https://doi.org/10.1016/j.atmosenv.2012.02.027, 2012.

Lauraguais, A., Bejan, I., Barnes, I., Wiesen, P., Coeur-Tourneur, C., and Cassez, A.: Rate coefficients for the gas-phase reaction of chlorine atoms with a series of methoxylated aromatic compounds, J. Phys. Chem. A, 118, 1777-1784, https://doi.org/10.1021/jp4114877, 2014a.

Lauraguais, A., Coeur-Tourneur, C., Cassez, A., Deboudt, K., Fourmentin, M., and Choel, M.: Atmospheric reactivity of hydroxyl radicals with guaiacol (2-methoxyphenol), a biomass burning emitted compound: Secondary organic aerosol formation and gas-phase oxidation products, Atmos. Environ., 86, 155-163, https://doi.org/10.1016/j.atmosenv.2013.11.074, 2014b.

Lauraguais, A., El Zein, A., Coeur, C., Obeid, E., Cassez, A., Rayez, M.-T., and Rayez, J.-C.: Kinetic study of the gas-phase reactions of nitrate radicals with methoxyphenol compounds: Experimental and theoretical approaches, J. Phys. Chem. A, 120, 2691-2699, https://doi.org/10.1021/acs.jpca.6b02729, 2016.

Lelieveld, J., Crutzen, P. J., Ramanathan, V., Andreae, M. O., Brenninkmeijer, C. A. M., Campos, T., Cass, G. R., Dickerson, R. R., Fischer, H., de Gouw, J. A., Hansel, A., Jefferson, A., Kley, D., de Laat, A. T. J., Lal, S., Lawrence, M. G., Lobert, J. M., Mayol-Bracero, O. L., Mitra, A. P., Novakov, T., Oltmans, S. J., Prather, K. A., Reiner, T., Rodhe, H., Scheeren, H. A., Sikka, D., and Williams, J.: The Indian Ocean Experiment: Widespread air pollution from South and Southeast Asia, Science, 291, 1031-1036, https://doi.org/10.1126/science.1057103, 2001.

Li, H., Zhang, Q., Zhang, Q., Chen, C., Wang, L., Wei, Z., Zhou, S., Parworth, C., Zheng, B., Canonaco, F., Prevot, A. S. H., Chen, P., Zhang, H., Wallington, T. J., and He, K.: Wintertime aerosol chemistry and haze evolution in an extremely polluted city of the North China Plain: Significant contribution from coal and biomass combustion, Atmos. Chem. Phys., 17, 4751-4768, https://doi.org/10.5194/acp-17-4751-2017, 2017.

Liggio, J., Li, S.-M., and McLaren, R.: Reactive uptake of glyoxal by particulate matter, J. Geophys. Res.-Atmos., 110, D10304, https://doi.org/10.1029/2004JD005113, 2005.

Lin, Y. H., Knipping, E. M., Edgerton, E. S., Shaw, S. L., and Surratt, J. D.: Investigating the influences of SO_2 and NH_3 levels on isoprene-derived secondary organic aerosol formation using conditional sampling approaches, Atmos. Chem. Phys., 13, 8457–8470, https://doi.org/10.5194/acp-13-8457-2013, 2013.

Liu, J., Lin, P., Laskin, A., Laskin, J., Kathmann, S. M., Wise, M., Caylor, R., Imholt, F., Selimovic, V., and Shilling, J. E.: Optical properties and aging of light-absorbing secondary organic aerosol, Atmos. Chem. Phys., 16, 12815-12827, https://doi.org/10.5194/acp-16-12815-2016, 2016a.

Liu, T., Wang, X., Hu, Q., Deng, W., Zhang, Y., Ding, X., Fu, X., Bernard, F., Zhang,

Z., Lu, S., He, Q., Bi, X., Chen, J., Sun, Y., Yu, J., Peng, P., Sheng, G., and Fu, J.: Formation of secondary aerosols from gasoline vehicle exhaust when mixing with SO_2, Atmos. Chem. Phys., 16, 675-689, https://doi.org/10.5194/acp-16-675-2016, 2016b.

Liu, Z., Ge, M., Yin, S., and Wang, W.: Uptake and reaction kinetics of α-pinene and β-pinene with sulfuric acid solutions, Chem. Phys. Lett., 491, 146-150, https://doi.org/10.1016/j.cplett.2010.04.004, 2010.

Marais, E. A., Jacob, D. J., Turner, J. R., and Mickley, L. J.: Evidence of 1991-2013 decrease of biogenic secondary organic aerosol in response to SO_2 emission controls, Environ. Res. Lett., 12, 054018, https://doi.org/10.1088/1748-9326/aa69c8, 2017.

Meade, L. E., Riva, M., Blomberg, M. Z., Brock, A. K., Qualters, E. M., Siejack, R. A., Ramakrishnan, K., Surratt, J. D., and Kautzman, K. E.: Seasonal variations of fine particulate organosulfates derived from biogenic and anthropogenic hydrocarbons in the mid-Atlantic United States, Atmos. Environ., 145, 405-414, https://doi.org/10.1016/j.atmosenv.2016.09.028, 2016.

Mielke, L. H., Furgeson, A., and Osthoff, H. D.: Observation of $ClNO_2$ in a mid-continental urban environment, Environ. Sci. Technol., 45, 8889-8896, https://doi.org/10.1021/es201955u, 2011.

Naeher, L. P., Brauer, M., Lipsett, M., Zelikoff, J. T., Simpson, C. D., Koenig, J. Q., and Smith, K. R.: Woodsmoke health effects: A review, Inhal. Toxicol., 19, 67-106, https://doi.org/10.1080/08958370600985875, 2007.

Ng, N. L., Chhabra, P. S., Chan, A. W. H., Surratt, J. D., Kroll, J. H., Kwan, A. J., McCabe, D. C., Wennberg, P. O., Sorooshian, A., Murphy, S. M., Dalleska, N. F., Flagan, R. C., and Seinfeld, J. H.: Effect of NO_x level on secondary organic aerosol (SOA) formation from the photooxidation of terpenes, Atmos. Chem. Phys., 7, 5159-5174, https://doi.org/10.5194/acp-7-5159-2007, 2007.

Ng, N. L., Canagaratna, M. R., Jimenez, J. L., Chhabra, P. S., Seinfeld, J. H., and Worsnop, D. R.: Changes in organic aerosol composition with aging inferred from aerosol mass spectra, Atmos. Chem. Phys., 11, 6465-6474, https://doi.org/10.5194/acp-11-6465-2011, 2011.

Nolte, C. G., Schauer, J. J., Cass, G. R., and Simoneit, B. R. T.: Highly polar organic compounds present in wood smoke and in the ambient atmosphere, Environ. Sci. Technol., 35, 1912-1919, https://doi.org/10.1021/es001420r, 2001.

O'Neill, E. M., Kawam, A. Z., Van Ry, D. A., and Hinrichs, R. Z.: Ozonolysis of surface-adsorbed methoxyphenols: kinetics of aromatic ring cleavage vs. alkene side-chain oxidation, Atmos. Chem. Phys., 14, 47-60, https://doi.org/10.5194/acp-14-47-2014, 2014.

Odum, J. R., Hoffmann, T., Bowman, F., Collins, D., Flagan, R. C., and Seinfeld, J. H.: Gas/particle partitioning and secondary organic aerosol yields, Environ. Sci. Technol., 30, 2580-2585, https://doi.org/10.1021/es950943+, 1996.

Park, J.-H., Ivanov, A. V., and Molina, M. J.: Effect of relative humidity on OH uptake

by surfaces of atmospheric importance, J. Phys. Chem. A, 112, 6968-6977, https://doi.org/10.1021/jp8012317, 2008.

Riva, M., Tomaz, So, Cui, T., Lin, Y. H., Perraudin, E., Gold, A., Stone, E. A., Villenave, E., and Surratt, J. D.: Evidence for an unrecognized secondary anthropogenic source of organosulfates and sulfonates: Gas-phase oxidation of polycyclic aromatic hydrocarbons in the presence of sulfate aerosol, Environ. Sci. Technol., 49, 6654−6664, https://doi.org/10.1021/acs.est.5b00836, 2015.

Sarrafzadeh, M., Wildt, J., Pullinen, I., Springer, M., Kleist, E., Tillmann, R., Schmitt, S. H., Wu, C., Mentel, T. F., Zhao, D., Hastie, D. R., and Kiendler-Scharr, A.: Impact of NO_x and OH on secondary organic aerosol formation from beta-pinene photooxidation, Atmos. Chem. Phys., 16, 11237-11248, https://doi.org/10.5194/acp-16-11237-2016, 2016.

Sato, K., Takami, A., Isozaki, T., Hikida, T., Shimono, A., and Imamura, T.: Mass spectrometric study of secondary organic aerosol formed from the photo-oxidation of aromatic hydrocarbons, Atmos. Environ., 44, 1080-1087, https://doi.org/10.1016/j.atmosenv.2009.12.013, 2010.

Schauer, J. J., Kleeman, M. J., Cass, G. R., and Simoneit, B. R. T.: Measurement of emissions from air pollution sources. 3. C-1-C-29 organic compounds from fireplace combustion of wood, Environ. Sci. Technol., 35, 1716-1728, https://doi.org/10.1021/es001331e, 2001.

Simoneit, B. R. T., Rogge, W. F., Mazurek, M. A., Standley, L. J., Hildemann, L. M., and Cass, G. R.: Lignin pyrolysis products, lignans, and resin acid as specific tracers of plant classes in emissions from biomass combustion, Environ. Sci. Technol., 27, 2533-2541, https://doi.org/10.1021/es00048a034, 1993.

Takekawa, H., Minoura, H., and Yamazaki, S.: Temperature dependence of secondary organic aerosol formation by photo-oxidation of hydrocarbons, Atmos. Environ., 37, 3413-3424, https://doi.org/10.1016/s1352-2310(03)00359-5, 2003.

Ulbrich, I. M., Canagaratna, M. R., Zhang, Q., Worsnop, D. R., and Jimenez, J. L.: Interpretation of organic components from Positive Matrix Factorization of aerosol mass spectrometric data, Atmos. Chem. Phys., 9, 2891-2918, https://doi.org/10.5194/acp-9-2891-2009, 2009.

Weis, D. D., and Ewing, G. E.: Water content and morphology of sodium chloride aerosol particles, J. Geophys. Res.-Atmos., 104, 21275-21285, https://doi.org/10.1029/1999jd900286, 1999.

Xu, L., Middlebrook, A. M., Liao, J., de Gouw, J. A., Guo, H., Weber, R. J., Nenes, A., Lopez-Hilfiker, F. D., Lee, B. H., Thornton, J. A., Brock, C. A., Neuman, J. A., Nowak, J. B., Pollack, I. B., Welti, A., Graus, M., Warneke, C., and Ng, N. L.: Enhanced formation of isoprene-derived organic aerosol in sulfur-rich power plant plumes during Southeast Nexus, J. Geophys. Res.-Atmos., 121, 11137-11153, https://doi.org/10.1002/2016jd025156, 2016.

Yang, B., Zhang, H., Wang, Y., Zhang, P., Shu, J., Sun, W., and Ma, P.: Experimental and theoretical studies on gas-phase reactions of NO_3 radicals with three

805   methoxyphenols: Guaiacol, creosol, and syringol, Atmos. Environ., 125, 243-251,
806   https://doi.org/10.1016/j.atmosenv.2015.11.028, 2016.

807 Ye, J., Abbatt, J. P. D., and Chan, A. W. H.: Novel pathway of SO_2 oxidation in the
808   atmosphere: reactions with monoterpene ozonolysis intermediates and secondary
809   organic aerosol, Atmos. Chem. Phys., 18, 5549-5565, https://doi.org/10.5194/acp-
810   18-5549-2018, 2018.

811 Yee, L. D., Kautzman, K. E., Loza, C. L., Schilling, K. A., Coggon, M. M., Chhabra, P.
812   S., Chan, M. N., Chan, A. W. H., Hersey, S. P., Crounse, J. D., Wennberg, P. O.,
813   Flagan, R. C., and Seinfeld, J. H.: Secondary organic aerosol formation from
814   biomass burning intermediates: Phenol and methoxyphenols, Atmos. Chem. Phys.,
815   13, 8019-8043, https://doi.org/10.5194/acp-13-8019-2013, 2013.

816 Zhang, X., Cappa, C. D., Jathar, S. H., McVay, R. C., Ensberg, J. J., Kleeman, M. J.,
817   and Seinfeld, J. H.: Influence of vapor wall loss in laboratory chambers on yields
818   of secondary organic aerosol, Proc. Natl. Acad. Sci. U. S. A., 111, 5802-5807,
819   https://doi.org/10.1073/pnas.1404727111, 2014.

820 Zhang, X., Schwantes, R. H., McVay, R. C., Lignell, H., Coggon, M. M., Flagan, R. C.,
821   and Seinfeld, J. H.: Vapor wall deposition in Teflon chambers, Atmos. Chem.
822   Phys., 15, 4197-4214, https://doi.org/10.5194/acp-15-4197-2015, 2015.

823 **Table 1.** Experimental conditions and results for guaiacol photoxidation in the presence

824 NO_x.

Exp.	[Guaiacol]$_0$	$\triangle$[Guaiacol]	[NO_x]$_0$	[NO]$_0$	RH	T	M_o	Yield
	($\mu g\ m^{-3}$)	($\mu g\ m^{-3}$)[a]	(ppbv)	(ppbv)	(%)	(K)	($\mu g\ m^{-3}$)[b]	(%)
1	136.83	112.34	25.1	13.2	39	302	10.63 ± 0.65	9.46 ± 1.71
2	309.06	282.33	52.7	34.4	38	302	34.72 ± 0.94	12.30 ± 0.98
3	375.19	335.94	58.3	44.5	40	302	63.62 ± 1.71	18.94 ± 1.49
4	718.49	613.25	116.7	98.5	38	302	130.19 ± 3.28	21.23 ± 1.56
5	1321.25	1116.20	209.2	184.1	39	302	256.88 ± 6.69	23.01 ± 1.75
6	1470.66	1175.03	248	200	38	302	297.65 ± 8.85	25.33 ± 2.21
7	2197.36	1664.29	335	286	38	302	438.82 ± 10.25	26.37 ± 2.83

825 [a] The consumed guaiacol concentration at the end of each experiment.

826 [b] M_o is the mass concentration of SOA.

827 **Table 2.** Experimental conditions and results for guaiacol photoxidation in the presence of seed particles and SO_2.

| Exp.	[Guaiacol]$_0$ ($\mu g\ m^{-3}$)	$\triangle$[Guaiacol] ($\mu g\ m^{-3}$)[a]	Seed	[SO$_2$]$_0$ (ppbv)	[NO$_x$]$_0$ (ppbv)	[NO]$_0$ (ppbv)	RH (%)	T (K)	N$_S$ (m^{-3})[b]	D$_S$ (nm)[c]	C$_{seed}$ ($\mu g\ m^{-3}$)[d]	C$_{sulfate}$ ($\mu g\ m^{-3}$)[e]	S$_0$ ($\mu m^2\ cm^{-3}$)[f]	S$_f$ ($\mu m^2\ cm^{-3}$)[g]	$\overline{\tau}_{g\text{-}p}/\tau_{g\text{-}w}$ h	M$_o$ ($\mu g\ m^{-3}$)[i]	Yield (%)	OS$_C$[j]
1	375.19	335.94	–	–	58.3	44.5	40	302	–	–	–	–	–	1.25×10^3	0.82	63.62 ± 1.71	18.94 ± 1.49	0.11 ± 0.007
2	363.53	332.79	–	33	54.5	37.4	38	302	–	–	–	7.42	–	1.68×10^3	0.71	71.88 ± 1.43	21.60 ± 1.27	0.14 ± 0.006
3	370.12	335.58	–	56	57.3	41.8	38	302	–	–	–	17.89	–	2.04×10^3	0.61	78.59 ± 2.06	23.42 ± 1.80	0.18 ± 0.006
4	379.05	346.03	NaCl	–	58.8	40.7	39	302	10700	56	15.63	–	2.69×10^2	1.47×10^3	0.54	84.91 ± 2.01	24.54 ± 1.73	0.29 ± 0.007
5	378.44	339.34	NaCl	30	57.4	41.9	38	302	11300	58	13.84	7.51	2.64×10^2	2.32×10^3	0.43	90.89 ± 2.28	26.78 ± 1.97	0.30 ± 0.008
6	380.77	340.15	NaCl	54	60.1	46.1	39	301	11200	56	14.28	16.67	2.81×10^2	2.91×10^3	0.35	98.86 ± 2.11	29.06 ± 1.82	0.33 ± 0.008
7	373.57	340.86	(NH$_4$)$_2$SO$_4$	–	58.3	42.6	39	302	10400	53	15.45	–	2.75×10^2	1.53×10^3	0.62	79.44 ± 1.86	23.31 ± 1.59	0.20 ± 0.006
8	376.26	343.19	(NH$_4$)$_2$SO$_4$	33	56.8	38.9	38	302	10100	53	14.38	7.84	2.80×10^2	2.57×10^3	0.53	84.35 ± 2.09	24.58 ± 1.78	0.22 ± 0.007
9	381.33	341.01	(NH$_4$)$_2$SO$_4$	54	57.8	39.2	38	303	10700	51	14.90	17.25	2.82×10^2	3.10×10^3	0.44	89.92 ± 2.31	26.37 ± 1.98	0.23 ± 0.004

828 [a] The consumed guaiacol concentration at the end of each experiment. [b] N_S is the initial seed number. [c] D_S is the average diameter of seed particles.

829 [d] C_{seed} is the initial concentration of seed. [e] $C_{sulfate}$ is the sulfate concentration formed by SO$_2$ oxidation. [f] The initial surface area of seed particles.

830 [g] The final surface area of aerosol particles (seed + organic aerosol), measured by the SMPS. [h] The ratio of the average gas-particle partitioning

831 timescale ($\overline{\tau}_{g\text{-}p}$) over the course of experiment to the vapor wall deposition timescale ($\tau_{g\text{-}w}$). [i] M_o is the mass concentration of SOA. [j] OS$_C$ is the

832 average oxidation state of carbon of SOA.

833
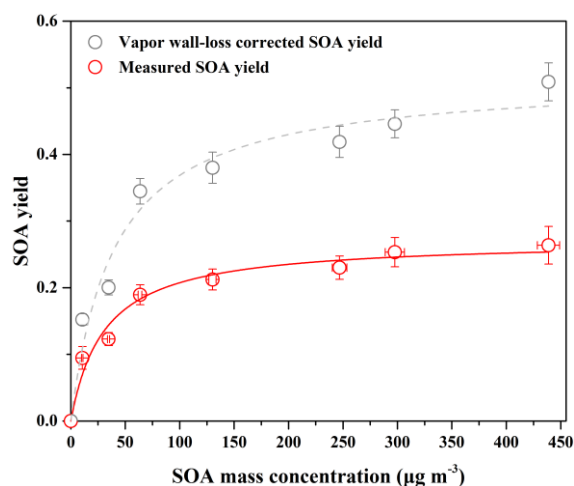
Figure 1. SOA yield as a function of SOA mass concentration (M_o) for guaiacol

photooxidation in the presence of NO_x at different guaiacol concentrations. The lines

were fit to the experimental data using a one-product model. Values of α and $K_{om,i}$ used

to generate the solid line were (0.27 $\pm$ 0.01) and (0.033 $\pm$ 0.008), and their values for

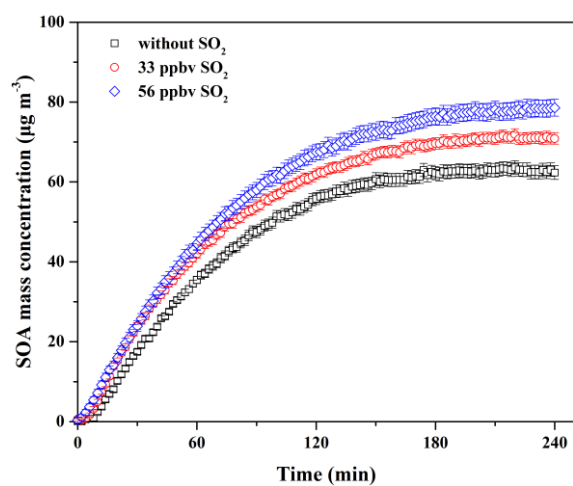the dot line were (0.52 $\pm$ 0.03) and (0.025 $\pm$ 0.006), respectively.

839

840 **Figure 2.** Time-dependent growth curves of SOA mass concentration for guaiacol

841 photooxidation at different SO_2 levels (Exps. 1−3 in Table 2).

842
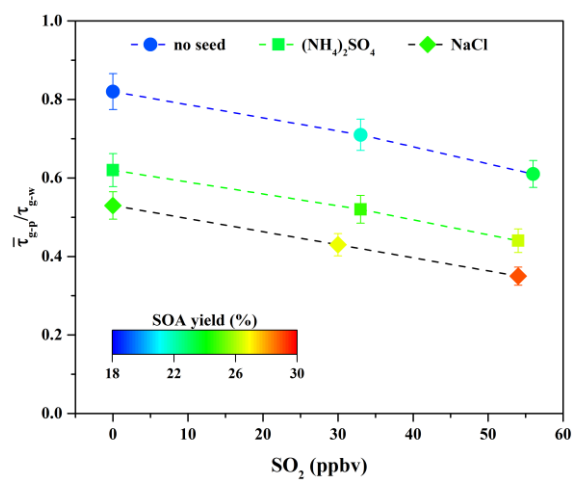
Figure 3. Variations in $\overline{\tau}_{g\text{-}p} / \tau_{g\text{-}w}$ ratio in the presence of various seed particles as a function of SO_2 concentration.
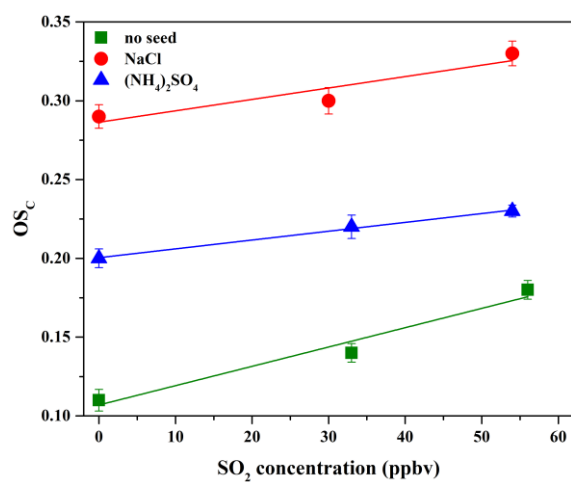
845
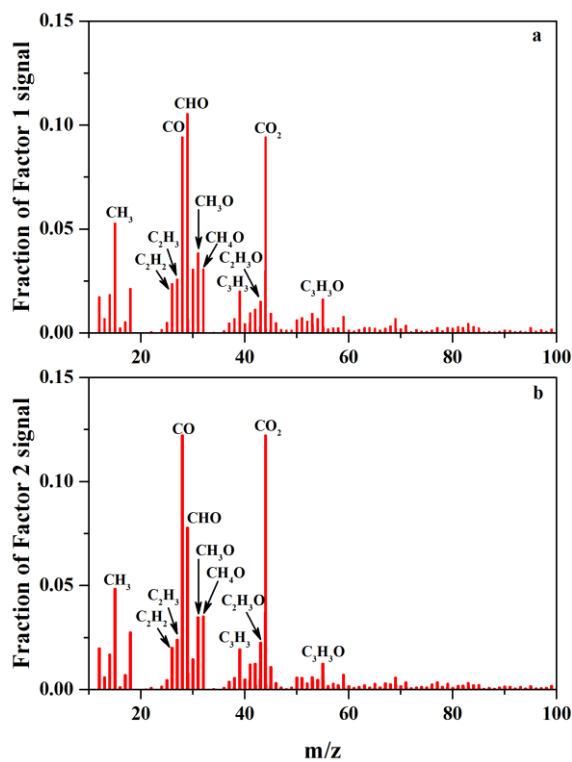
Figure 4. Mass spectra of Factor 1 (a) and Factor 2 (b) for the formed SOA identified

by applying PMF analysis to the AMS data, obtained at different SO_2 concentrations

over the courses of experiments.

849

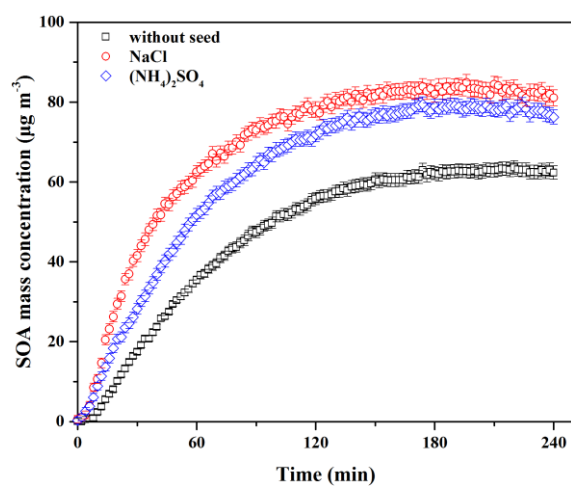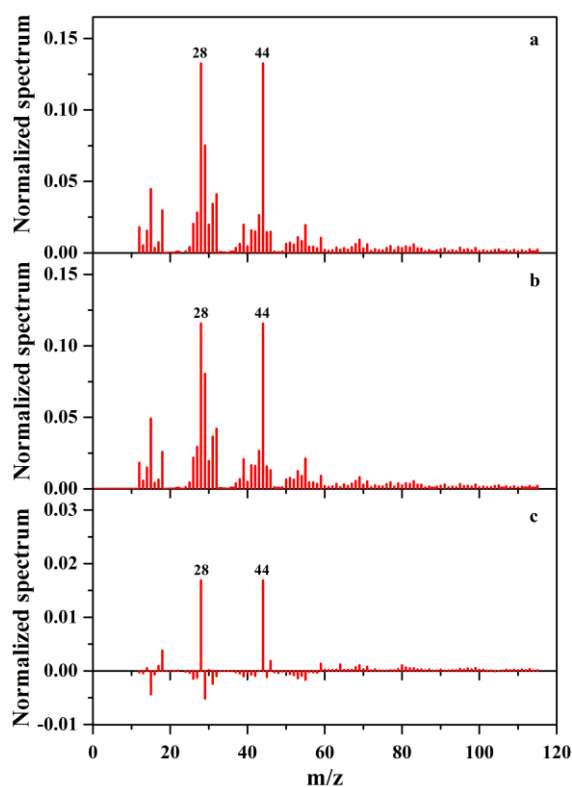**Figure 5.** OS_C of SOA formed in the presence of various seed particles as a function of SO_2 concentration.

852

Figure 6. Time-dependent growth curves of SOA mass concentration for guaiacol

photooxidation in the presence of inorganic seed particles (Exps. 1, 4 and 7 in Table 2).

855

Figure 7. Mass spectra of SOA with NaCl (a) and $(NH_4)_2SO_4$ (b) as seed particles

obtained by the HR-ToF-AMS, as well as their difference mass spectrum (c) obtained
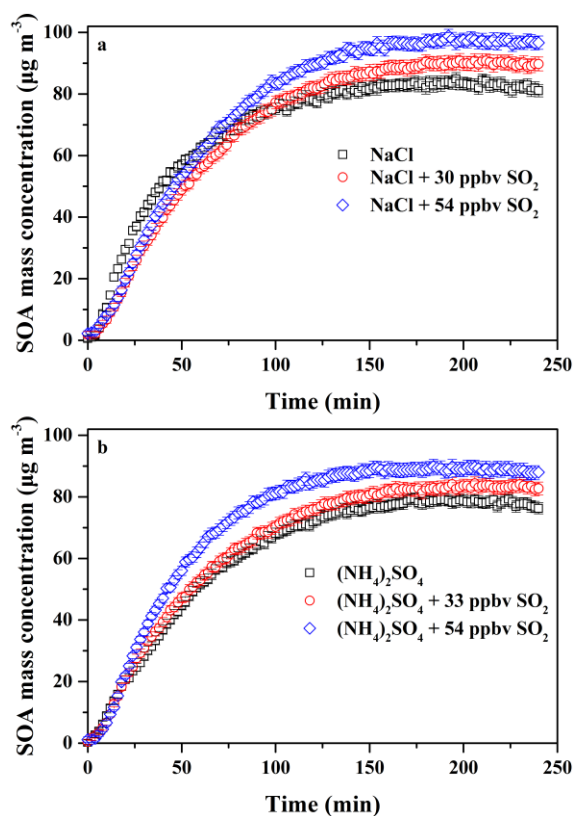
by a minus b.

859

Figure 8. Time-dependent growth curves of SOA mass concentration for guaiacol photooxidation in the presence of SO_2 and inorganic seed particles (a: NaCl; b: $(NH_4)_2SO_4$) (Exps. 4−9 in Table 2).